Supplementary information

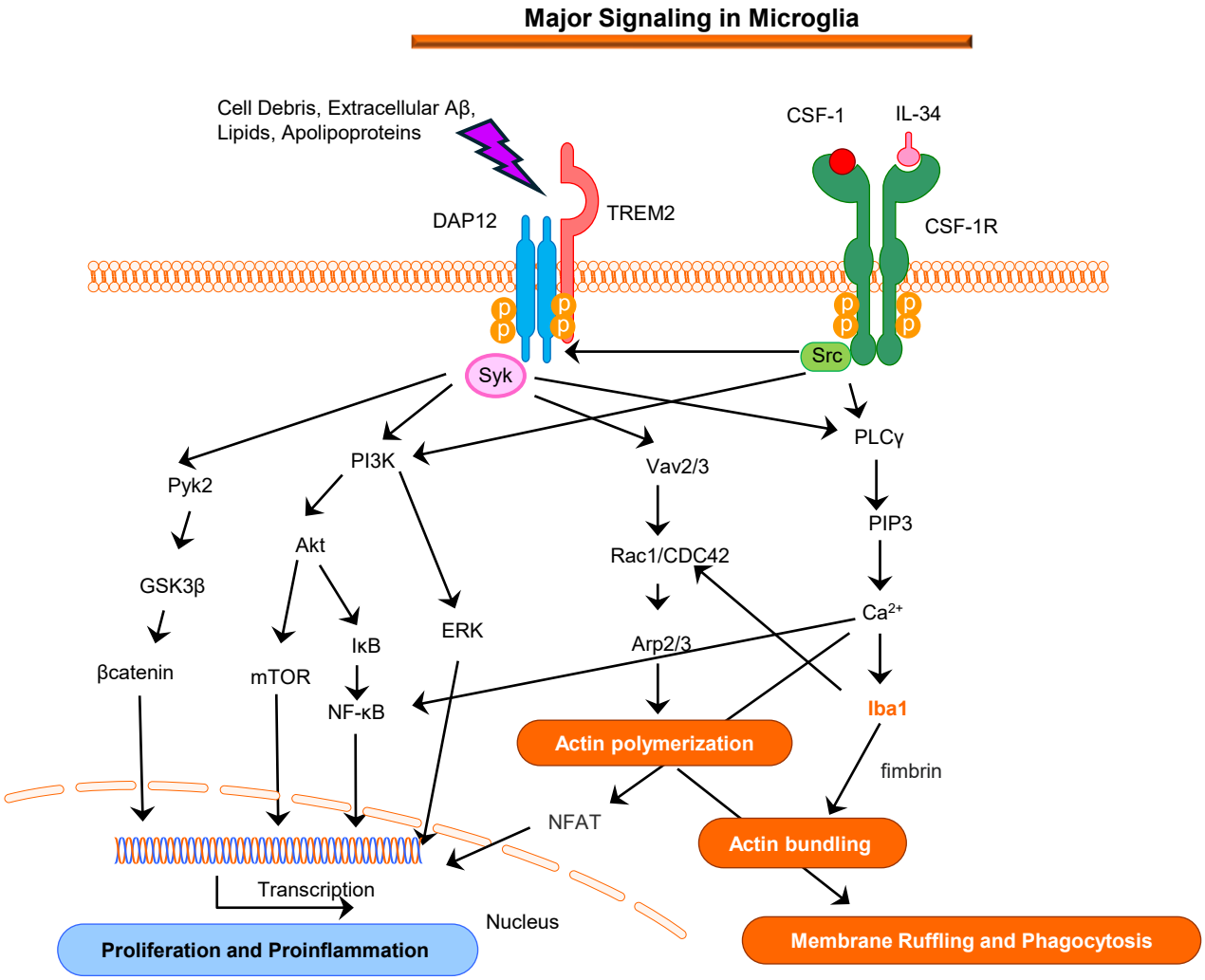

Figure S1. Iba1-mediated regulation of microglial signaling and actin dynamics.
Activation of Fc receptors or TREM2 triggers phosphorylation cascades that recruit kinases and induce NFAT-mediated transcription. In parallel, Iba1 interacts with fimbrin to promote actin polymerization and bundling, thereby facilitating membrane ruffling and phagocytosis.
Aβ, Amyloid-β peptide; Akt (PKB), Protein kinase B; Arp2/3, Actin-Related Protein 2/3 complex; Ca^{2+}, Calcium ion; CSF-1 (CSF1/M-CSF), Colony-Stimulating Factor-1; CSF1R, Colony-Stimulating Factor-1 Receptor; DAP12, DNAX-Activating Protein of 12 kDa; ERK (MAPK/ERK), Extracellular signal-regulated kinase (ERK1/2); GSK3β, Glycogen Synthase Kinase-3 beta; Iba1 (AIF1), Ionized calcium-binding adaptor molecule-1; IκB, Inhibitor of NF-κB; IL-34, Interleukin-34; mTOR, mechanistic Target of Rapamycin; NFAT, Nuclear Factor of Activated T-cells; NF-κB, Nuclear Factor kappa-B; PI3K, Phosphoinositide 3-kinase; PIP3, Phosphatidylinositol-3,4,5-trisphosphate; PLCγ, Phospholipase C gamma; Pyk2 (PTK2B), Proline-rich tyrosine kinase-2; RAC1, Ras-related C3 botulinum toxin substrate-1; SRC, Proto-oncogene tyrosine-protein kinase Src; SYK, Spleen Tyrosine Kinase; TREM2, Triggering Receptor Expressed on Myeloid Cells-2; Vav2/3 (VAV2/VAV3), Rho-family guanine-nucleotide exchange factors (GEFs).

a

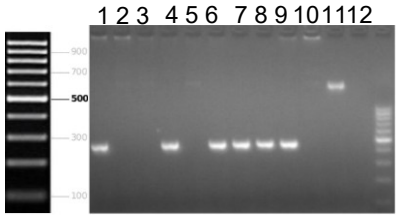

b

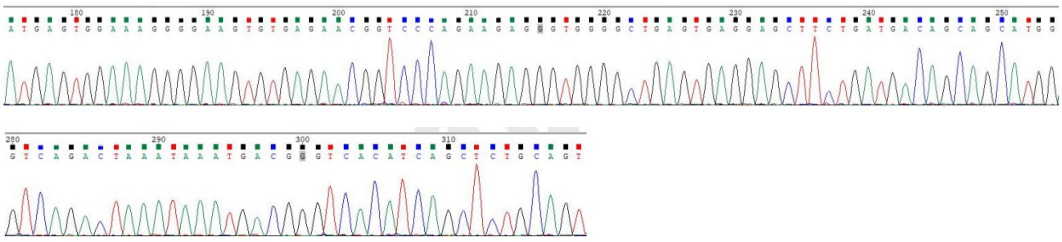

Figure S2. Generation of Iba1-deficient mice (Iba1$^{-/-}$).
(a) Genotyping was performed using a PCR-based assay, yielding a 1996 bp fragment for the wild-type (*Iba1*$^{+/+}$) allele and a 466 bp fragment for the targeted allele. Genotyping results for *Iba1*$^{-/-}$ mice are displayed in lanes 1, 4, 6, 7, 8, and 9, with lane 11 representing the *Iba1*$^{+/+}$ control and lane 12 serving as the no-template control.
(b) Results of Sanger sequencing analysis.

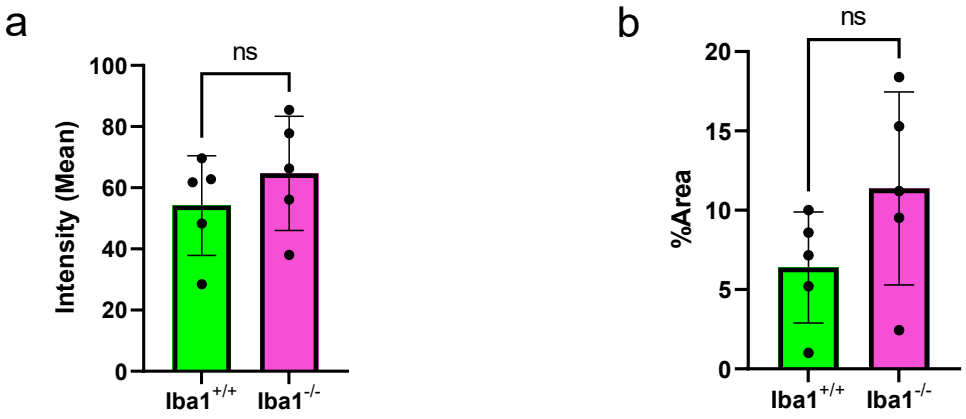

Figure S3. Quantification of cortical P2RY12 immunoreactivity in 8-week-old *Iba1*$^{+/+}$ and *Iba1*$^{-/-}$ mice.
(a) P2RY12 fluorescence intensity. (b) P2RY12-positive area fraction. Neither measure differed significantly between genotypes. Data are presented as mean ± standard error of the mean.

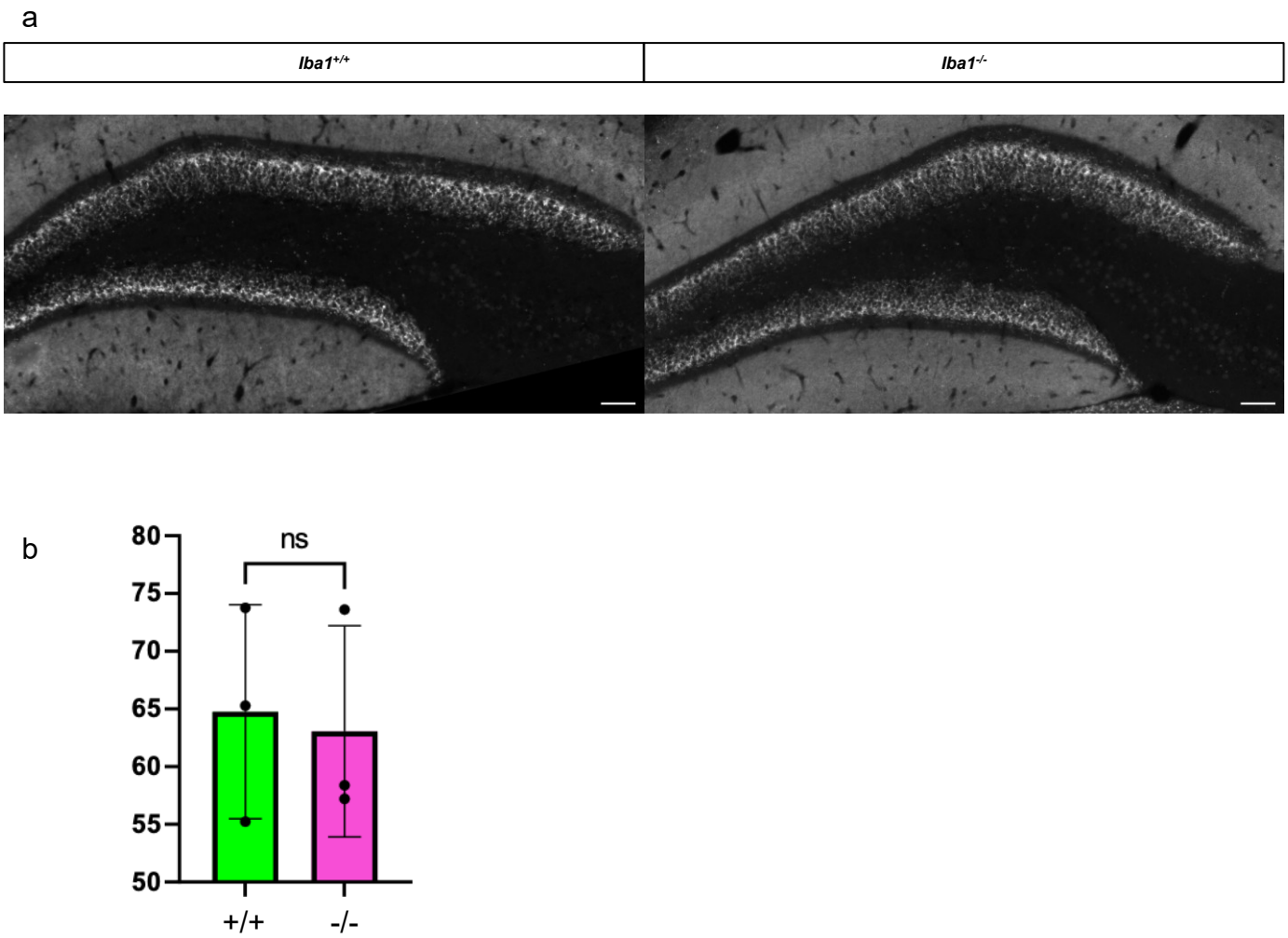

Figure S4. Hippocampus dentate gyrus VGLUT2 immunolabeling and fluorescence intensity in 8-week-old *Iba1*$^{+/+}$ and *Iba1*$^{-/-}$ mice.
(a) Representative images of the hippocampal formation from *Iba1*$^{+/+}$ and *Iba1*$^{-/-}$ mice immunostained for VGLUT2 at postnatal week 8. Scale bar: 20 µm. (b) Quantification of VGLUT2 fluorescence intensity within ROIs. Mean fluorescence intensity (MFI) was background-subtracted. Each dot represents one mouse; bars indicate mean ± SD (*Iba1*$^{+/+}$, n = 3; *Iba1*$^{-/-}$, n = 3). Statistical comparison used a two-tailed unpaired t-test (or Mann–Whitney U if non-normality); exact P values are shown, with no significance indicated.

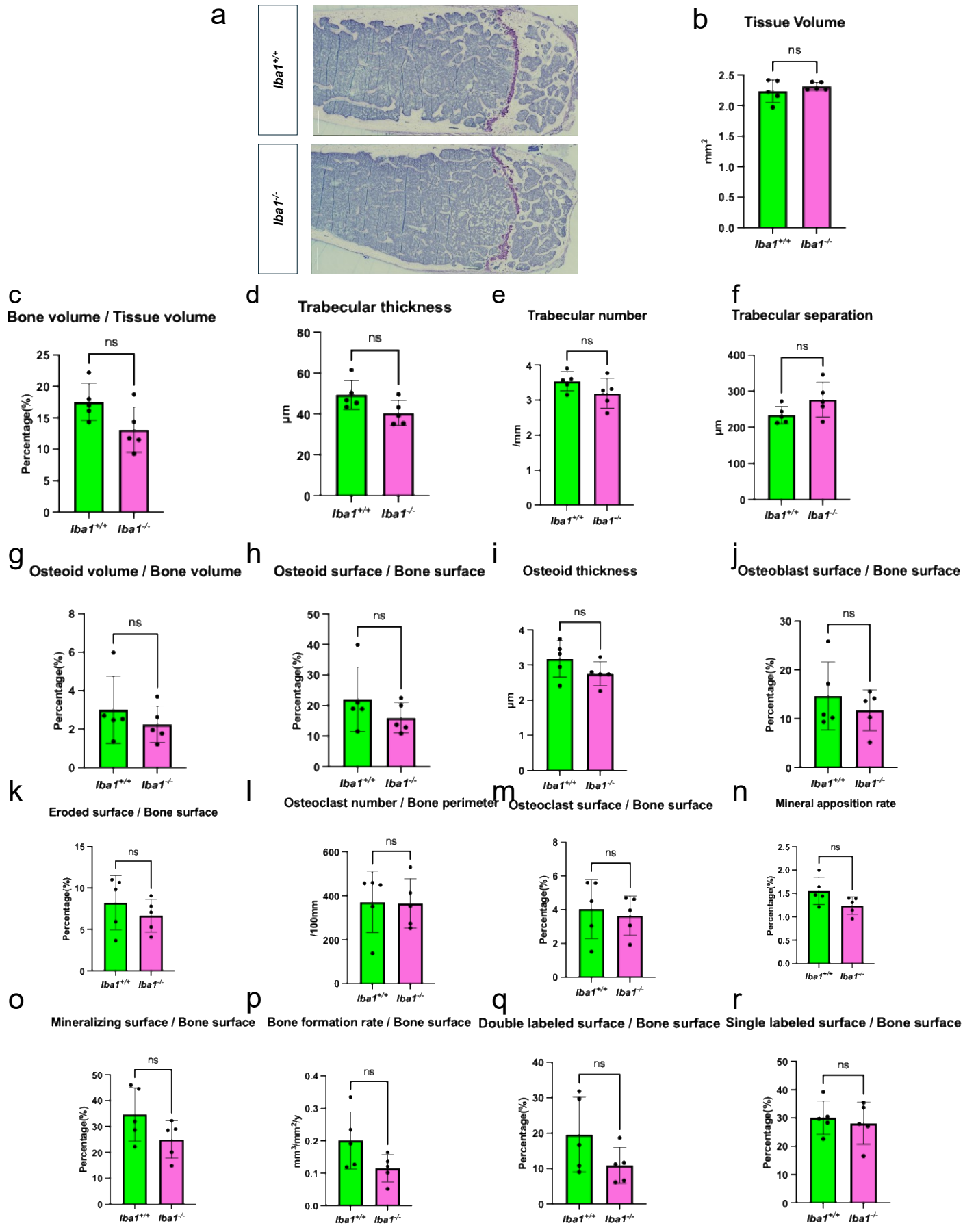

Figure S5. Bone histomorphometry

(a) Representative histology. Undecalcified long-bone metaphysis stained with toluidine blue, illustrating the trabecular region analyzed. Scale bar = 500 µm.
(b–r) Quantitative histomorphometry. Mean ± SEM; *Iba1*$^{+/+}$ n = 5 , *Iba1*$^{-/-}$ n = 5 ; green = *Iba1*$^{+/+}$, magenta = *Iba1*$^{-/-}$. Parameters follow ASBMR nomenclature and axis units:
(b) Tissue volume (TV, mm²) , (c) Bone volume / Tissue volume (BV/TV, %), (d) Trabecular thickness (Tb.Th, µm), (e) Trabecular number (Tb.N, /mm), (f) Trabecular separation (Tb.Sp, µm), (g) Osteoid volume / Bone volume (OV/BV, %), (h) Osteoid surface / Bone surface (OS/BS, %), (i) Osteoid thickness (O.Th, µm), (j) Osteoblast surface / Bone surface (Ob.S/BS, %), (k) Eroded surface / Bone surface (ES/BS, %), (l) Osteoclast number / Bone perimeter (N.Oc/B.Pm, /100 mm), (m) Osteoclast surface / Bone surface (Oc.S/BS, %), (n) Mineral apposition rate (MAR, µm/day), (o) Mineralizing surface / Bone surface (MS/BS, %), (p) Bone formation rate / Bone surface (BFR/BS, mm³/mm²/year), (q) Double-labeled surface / Bone surface (dLS/BS, %), (r) Single-labeled surface / Bone surface (sLS/BS, %).

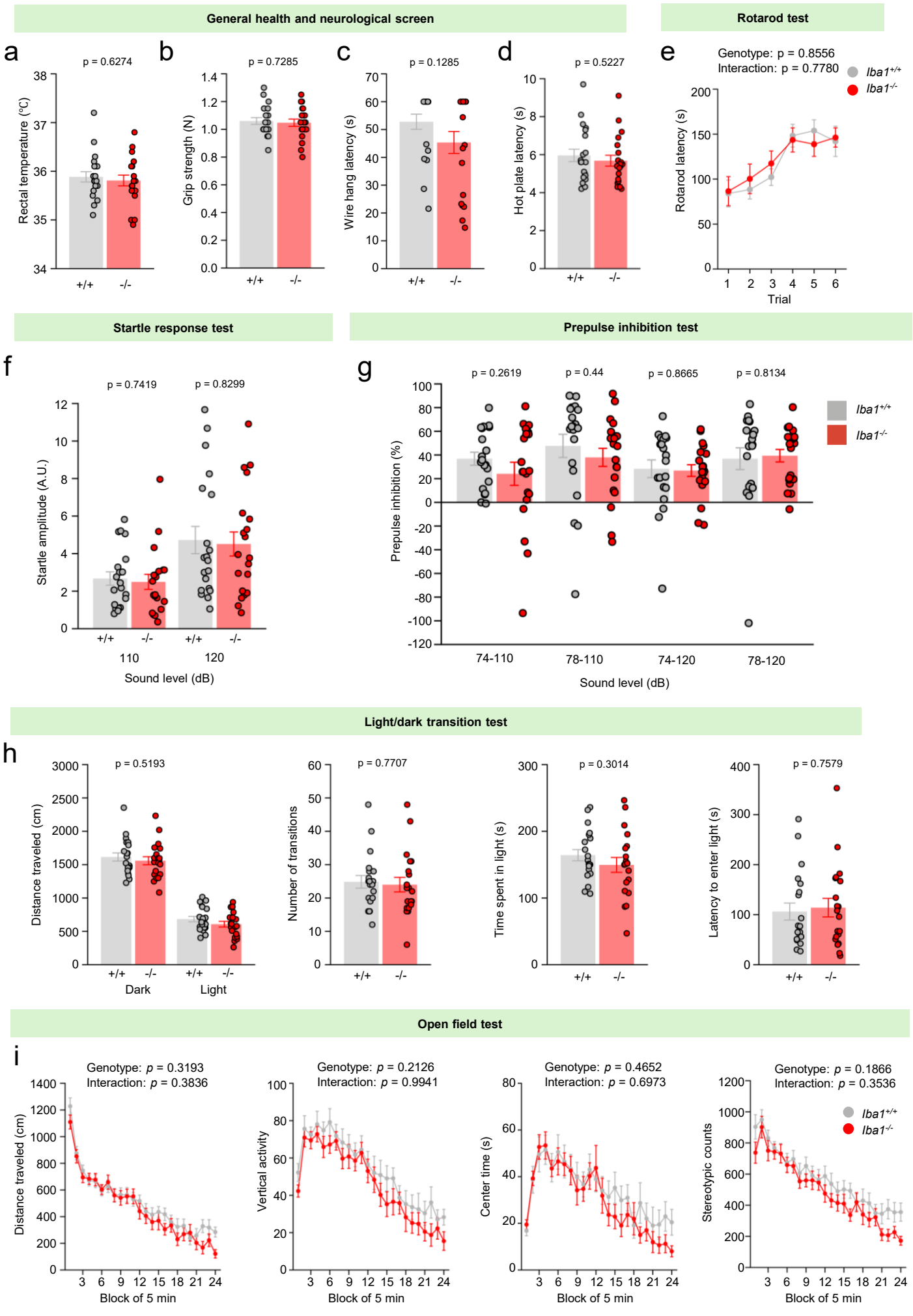
General health and neurological screen
Rotarod test
a
p = 0.6274
Rectal temperature (°C)
38
37
36
35
34
+/+
-/-
b
p = 0.7285
Grip strength (N)
1.4
1.2
1.0
0.8
0.6
0.4
0.2
0.0
+/+
-/-
c
p = 0.1285
Wire hang latency (s)
70
60
50
40
30
20
10
0
+/+
-/-
d
p = 0.5227
Hot plate latency (s)
10
8
6
4
2
0
+/+
-/-
e
Genotype: p = 0.8556
Interaction: p = 0.7780
lba1+/+
lba1-/-
Rotarod latency (s)
200
150
100
50
0
1
2
3
4
5
6
Trial
Startle response test
Prepulse inhibition test
f
p = 0.7419
p = 0.8299
Startle amplitude (A.U.)
12
10
8
6
4
2
0
+/+
-/-
+/+
-/-
110
120
Sound level (dB)
g
p = 0.2619
p = 0.44
p = 0.8665
p = 0.8134
Prepulse inhibition (%)
100
80
60
40
20
0
-20
-40
-60
-80
-100
-120
74-110
78-110
74-120
78-120
Sound level (dB)
lba1+/+
lba1-/-
Light/dark transition test
h
p = 0.5193
Distance traveled (cm)
3000
2500
2000
1500
1000
500
0
+/+
-/-
+/+
-/-
Dark
Light
p = 0.7707
Number of transitions
60
50
40
30
20
10
0
+/+
-/-
p = 0.3014
Time spent in light (s)
300
200
100
0
+/+
-/-
p = 0.7579
Latency to enter light (s)
400
300
200
100
0
+/+
-/-
Open field test
i
Genotype: p = 0.3193
Interaction: p = 0.3836
Distance traveled (cm)
1400
1200
1000
800
600
400
200
0
3
6
9
12
15
18
21
24
Block of 5 min
Genotype: p = 0.2126
Interaction: p = 0.9941
Vertical activity
100
80
60
40
20
0
3
6
9
12
15
18
21
24
Block of 5 min
Genotype: p = 0.4652
Interaction: p = 0.6973
Center time (s)
80
60
40
20
0
3
6
9
12
15
18
21
24
Block of 5 min
Genotype: p = 0.1866
Interaction: p = 0.3536
Stereotypic counts
1200
1000
800
600
400
200
0
3
6
9
12
15
18
21
24
Block of 5 min
lba1+/+
lba1-/-

Figure S6. Neurological health, acoustic startle response, sensorimotor gating, and locomotor/anxiety-related behaviors.
(a–d) General health and neurological screen: rectal temperature, forelimb grip strength, wire-hang latency, and hot-plate latency in *Iba1*$^{+/+}$ and *Iba1*$^{-/-}$ mice.
(e) Rotarod latency to fall from an accelerating rod across trials.
(f) Acoustic startle response to 110- and 120-dB white-noise pulses.
(g) Prepulse inhibition at 74- and 78-dB prepulses.
(h) Light–dark transition test: distance traveled in the dark and light chambers, number of transitions, time spent in the light chamber, and latency to first entry into the light chamber.
(i) Open field test: distance traveled, vertical activity, center time, and stereotypy counts across 5-min bins.
Data are expressed as mean ± standard error of the mean; *Iba1*$^{+/+}$ (open symbols/bars, $n = 20$) and *Iba1*$^{-/-}$ (filled symbols/bars, $n = 20$). Between-genotype comparisons of single endpoints were performed using unpaired two-tailed Student's *t*-test. Time- and trial-dependent measures (rotarod, startle/PPI, and open field) were analyzed using two-way repeated-measures analysis of variance (genotype × time or genotype × stimulus level). No significant genotype effects were detected; exact *p*-values are shown in the panels where applicable.

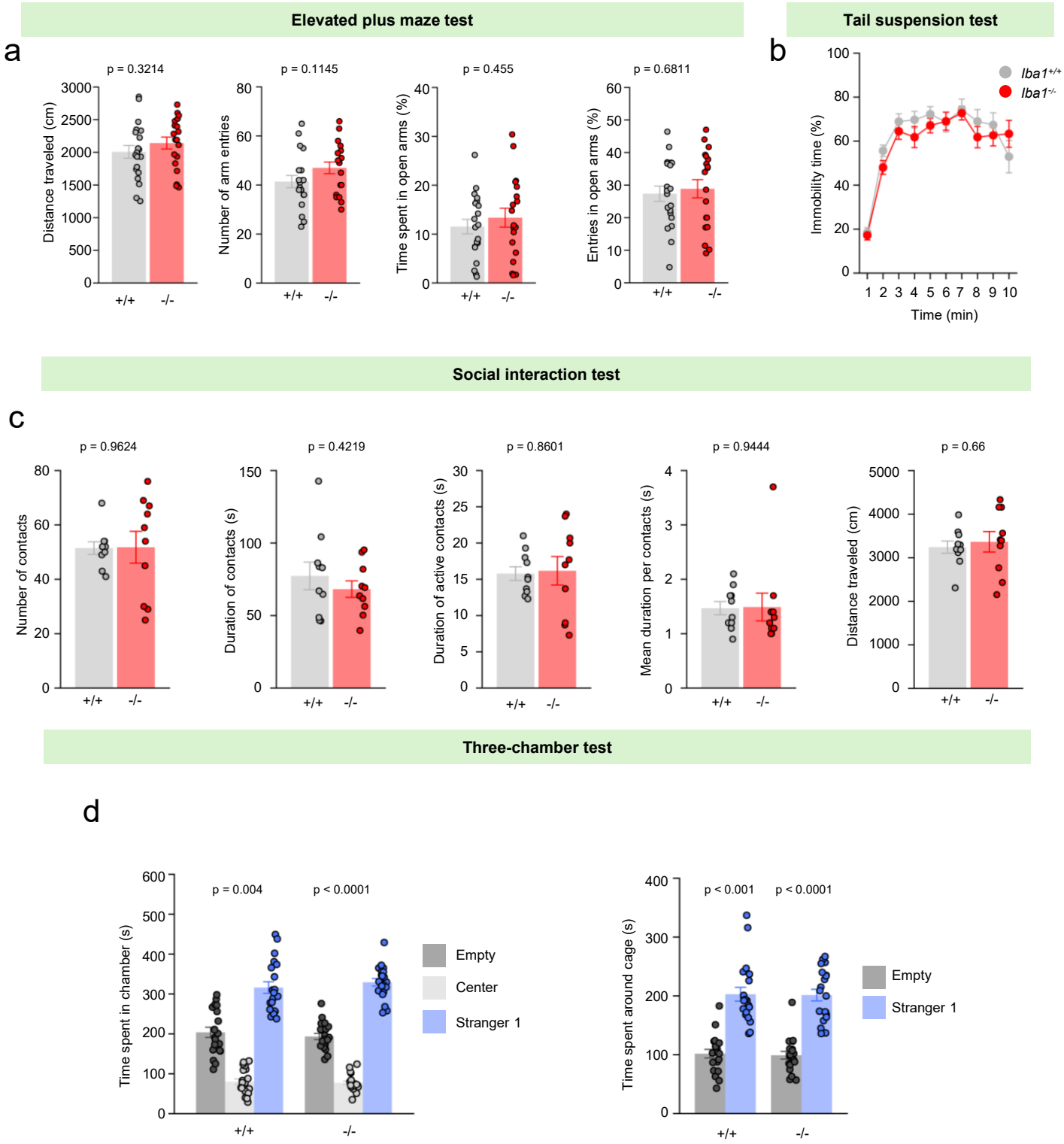

Figure S7. Anxiety-like, depression-like, and social behaviors.
(a) Elevated plus maze test: distance traveled, total arm entries, percentage of time spent in open arms, and percentage of open-arm entries.
(b) Tail suspension test: immobility (%) across 1-min bins.
(c) Social interaction test in a novel arena: number of contacts, total contact duration, active contact duration, mean duration per contact, and distance traveled.
(d) Three-chamber sociability test: time spent in each chamber (empty, center, and stranger 1) and time around empty vs. stranger 1 cages; both genotypes preferentially explored stranger 1, indicating preserved sociability. Data are expressed as mean ± standard error of the mean; *Iba1*$^{+/+}$ (open bars/symbols, $n = 20$) and *Iba1*$^{-/-}$ (filled bars/symbols, $n = 20$). Group comparisons for elevated plus maze, tail suspension (overall genotype effect), social interaction, and three-chamber sociability tests were performed using unpaired two-tailed Student's *t*-tests. Time-binned measures (tail suspension) were analyzed using two-way repeated-measures analysis of variance (genotype × time). Within-genotype sociability preferences (empty vs. stranger 1) were assessed using two-tailed paired *t*-tests. No significant genotype effects were observed; *p*-values are indicated in the panels where relevant.

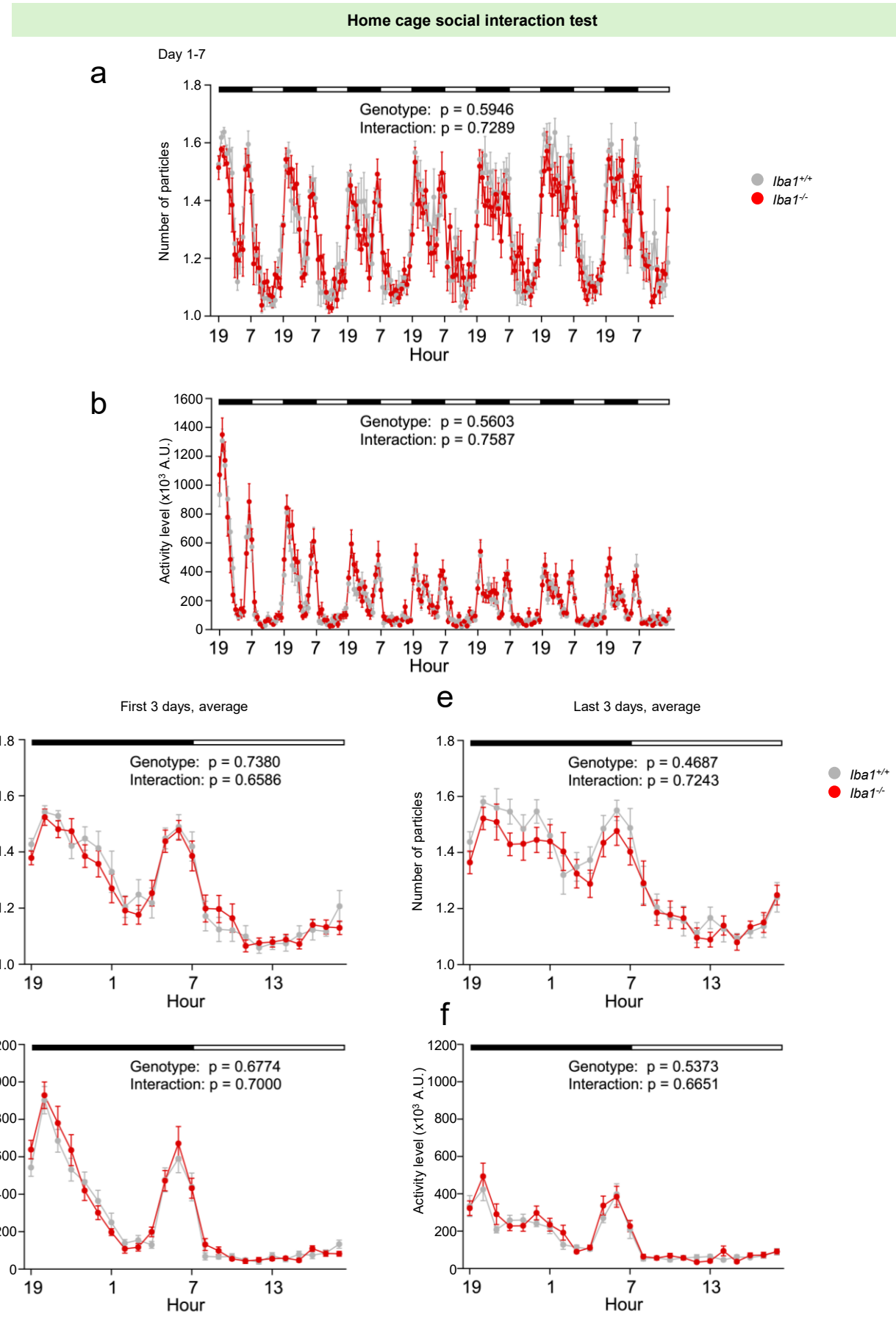

Figure S8. Home-cage circadian activity in *Iba1*$^{-/-}$ mice.
(a,b) Continuous home-cage monitoring of particle number and activity level over multiple days in *Iba1*$^{+/+}$ and *Iba1*$^{-/-}$ mice (n = 10 per genotype). Activity rhythms aligned with the light–dark cycle.
(c–f) Phase-averaged 24-h profiles of particle number (c,e) and activity level (d,f) during the first 3 days and last 3 days after cage placement.
Data are presented as mean ± standard error of the mean. Statistical analysis was performed using two-way repeated-measures analysis of variance (genotype × time). No significant genotype main effects or genotype × time interactions were detected (panel p-values shown), indicating intact baseline locomotor activity and circadian rhythmicity.

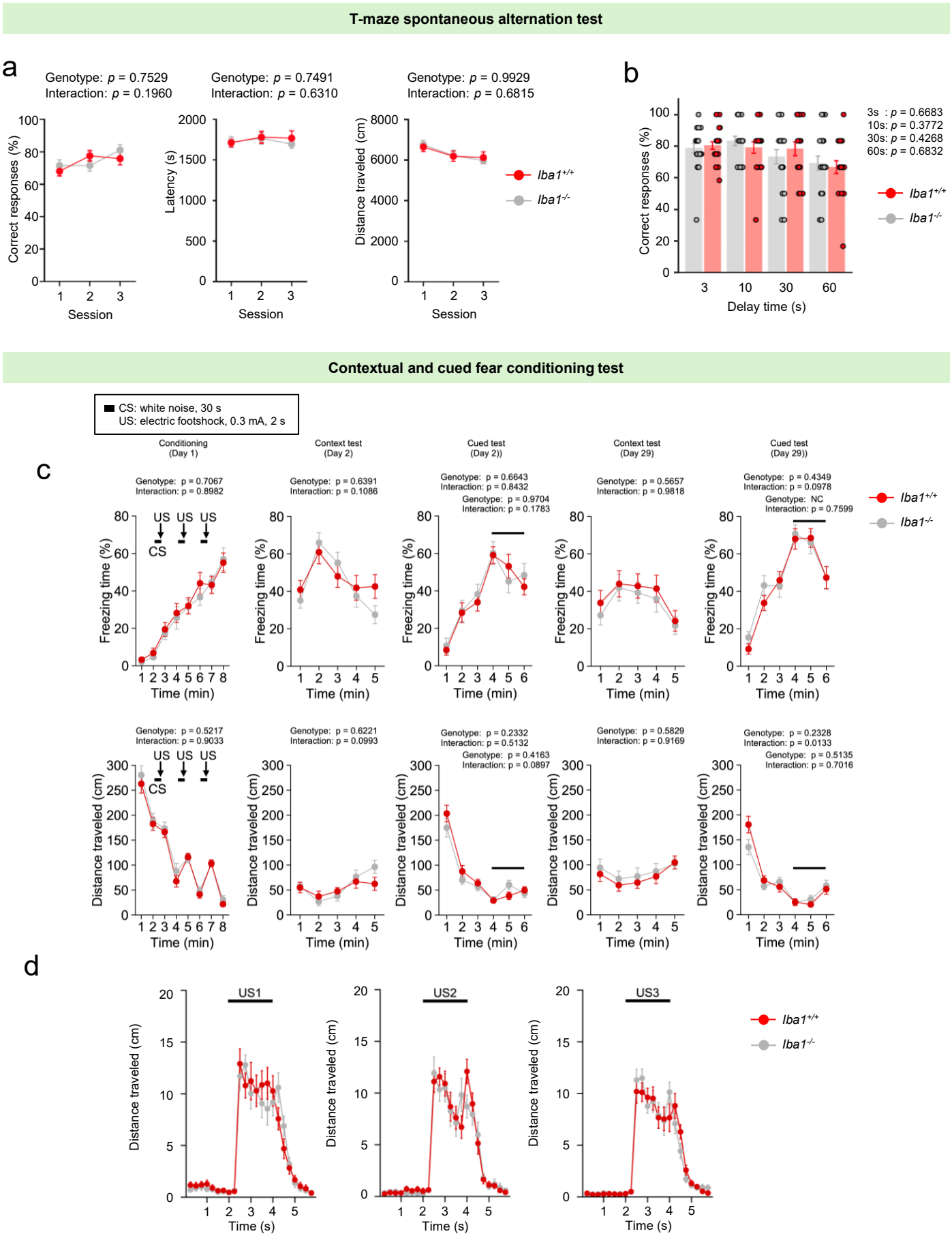

Figure S9. Working memory and fear conditioning in *Iba1*$^{-/-}$ mice.
(a,b) T-maze delayed alternations. *Iba1*$^{+/+}$ and *Iba1*$^{-/-}$ mice (n = 20 per genotype) were tested across three sessions and delay periods (3, 10, 30, and 60 s). Correct response rate, latency to complete the session, and distance traveled did not differ between genotypes.
(c) Contextual and cued fear conditioning. Freezing (%) during conditioning and during context and cued tests 1 and 28 days after conditioning.
(d) Acute shock responses: distance traveled within 6-s windows around footshocks (US1–US3).
Data are expressed as mean ± standard error of the mean. T-maze and fear-conditioning measures were analyzed by two-way repeated-measures analysis of variance (ANOVA) with genotype and time (or delay) as factors. No significant genotype main effects or genotype × time interactions were detected unless indicated by panel p-values.

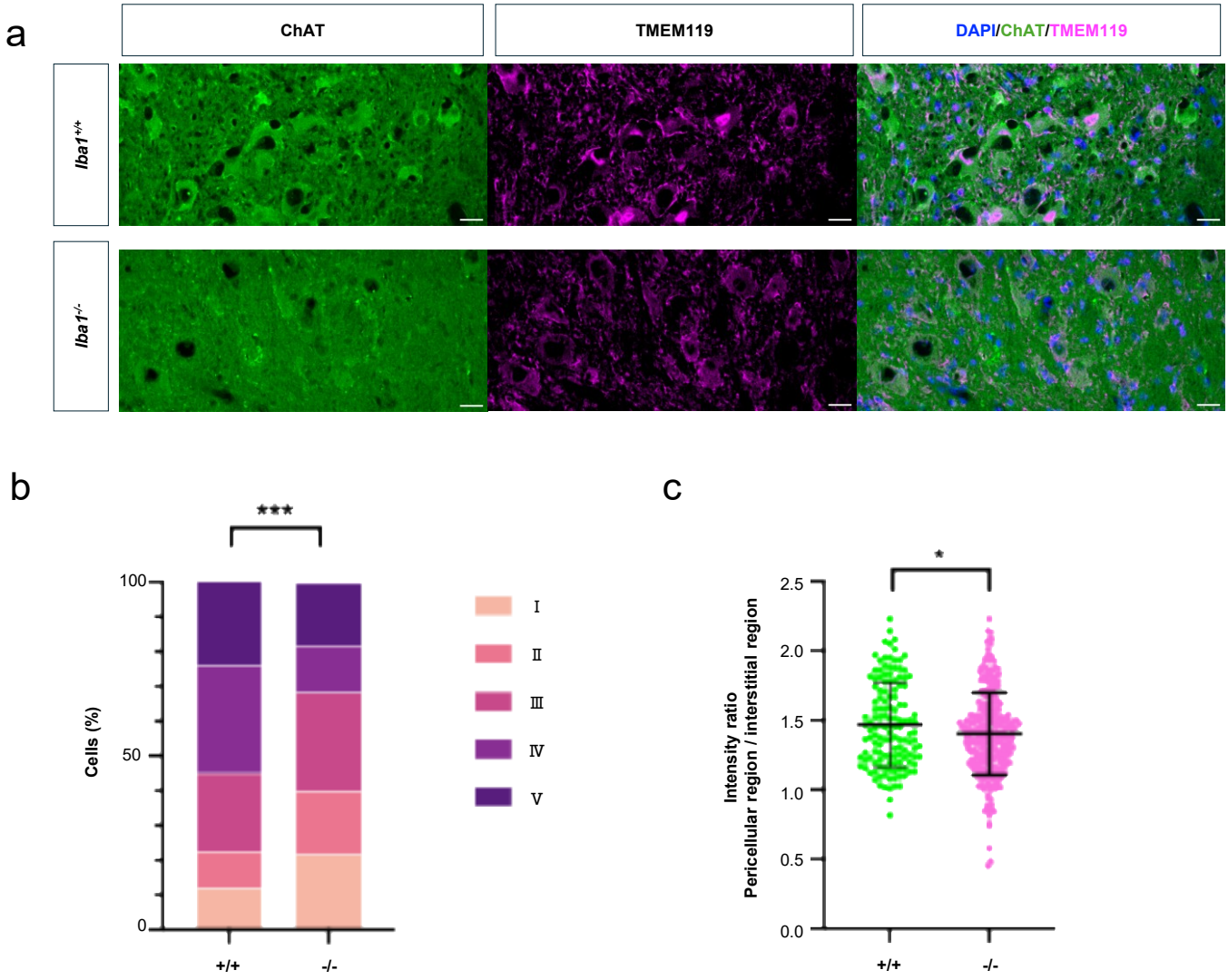

Figure S10. Quantification of TMEM119 perineuronal microglia 7 days post–facial nerve axotomy in *Iba1* wild-type and knockout mice.
(a) Representative immunofluorescence images showing ChAT (green) and TMEM119 (magenta) in axotomized and contralateral sides of *Iba1*$^{+/+}$ and *Iba1*$^{-/-}$ mice. Scale bars: 20 µm.
(b) Proportion of cells in each synaptic-stripping category, as classified in Fig. 3b. Data represent four animals per group (*Iba1*$^{+/+}$, n = 136 cells; *Iba1*$^{-/-}$, n = 146 cells). A significant difference was observed between the groups (chi-square test, ****$p < 0.0001$).
(c) Scatter plot showing the ratio of TMEM119 fluorescence intensity around neuronal somata normalized to the background TMEM119 intensity. *Iba1*$^{+/+}$ (yellow-green), *Iba1*$^{-/-}$ (magenta). ****$p < 0.0001$ where indicated.

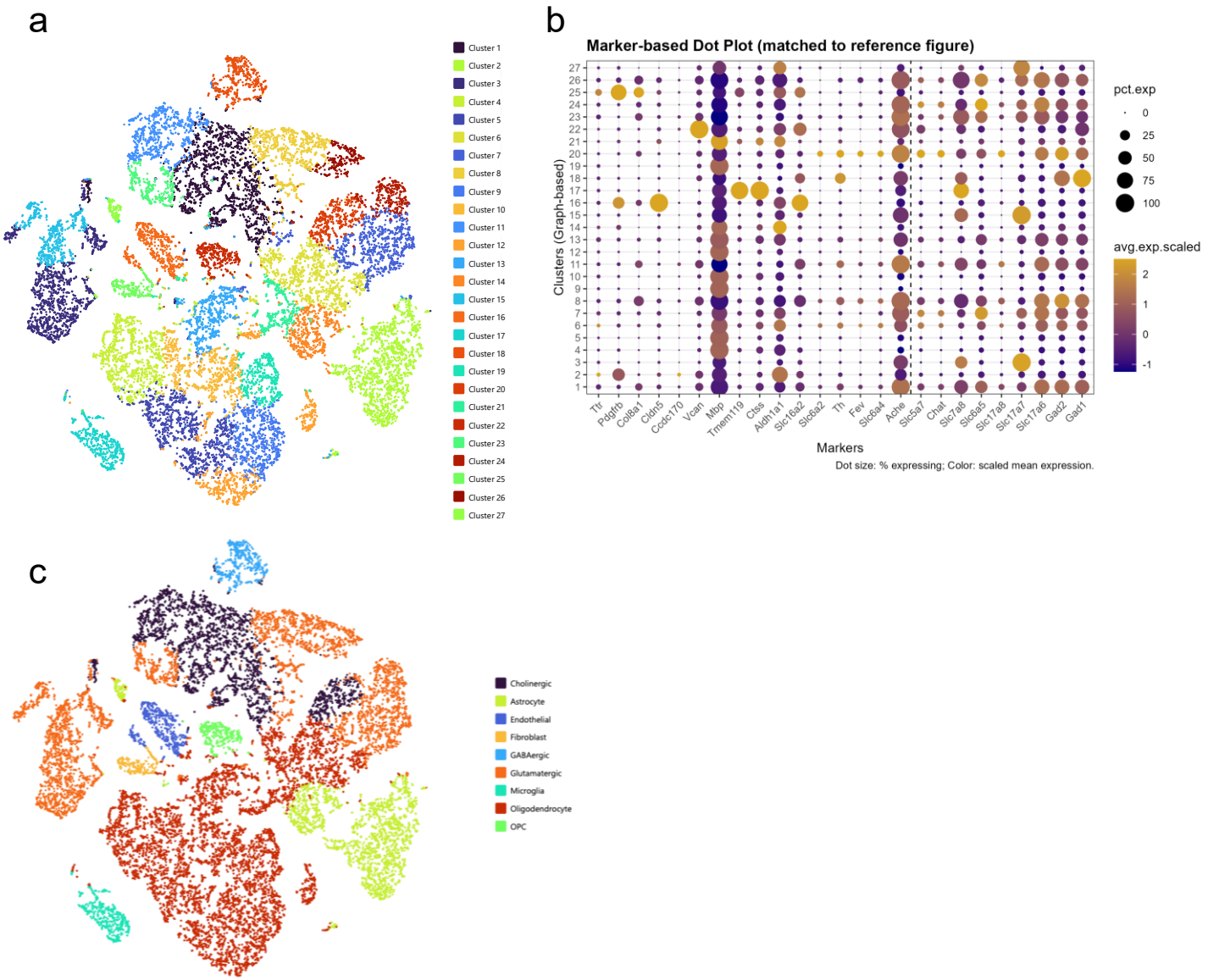

Figure S11. Marker-based dot plot across graph-based clusters.
(a) t-SNE of all nuclei partitioned by graph-based clustering into 27 clusters (GraphClust 1–27).
(b) Dot plot showing canonical neuronal and non-neuronal markers across GraphClust 1–27. Neuronal rows include GABAergic (Gad1, Gad2), glutamatergic (Slc17a6, Slc17a7, Slc17a8), glycinergic (Slc6a5, Slc7a8), and cholinergic (Chat, Slc5a7, Ache) markers; modulatory neuron markers (serotonergic: Slc6a4, Fev; dopaminergic: Th, Slc18a2; noradrenergic: Slc6a2, Th) are shown for reference. Non-neuronal rows include astrocyte (Aldh1a1), microglia (Ctss, Tmem119), oligodendrocyte (Mbp), OPC (Vcan), endothelial (Cldn5), fibroblast (Col8a1), ependymal (Ccdc170), pericyte (Pdgfrb), and choroid plexus (Ttr) markers. Dot size indicates the percentage of expressing nuclei; color indicates gene-wise scaled mean expression (z-score). A dashed line separates neuronal from non-neuronal marker blocks.
(c) Cell-type assignments derived from the marker profiles in (b). Clusters were annotated as glutamatergic, GABAergic, glycinergic, or cholinergic neurons; astrocytes, microglia, oligodendrocytes, OPCs; endothelial cells; and fibroblasts. Serotonergic and noradrenergic neuronal classes, as well as ependymal cells, pericytes, and choroid plexus cells, were not detected in this dataset based on absent/low canonical marker enrichment.

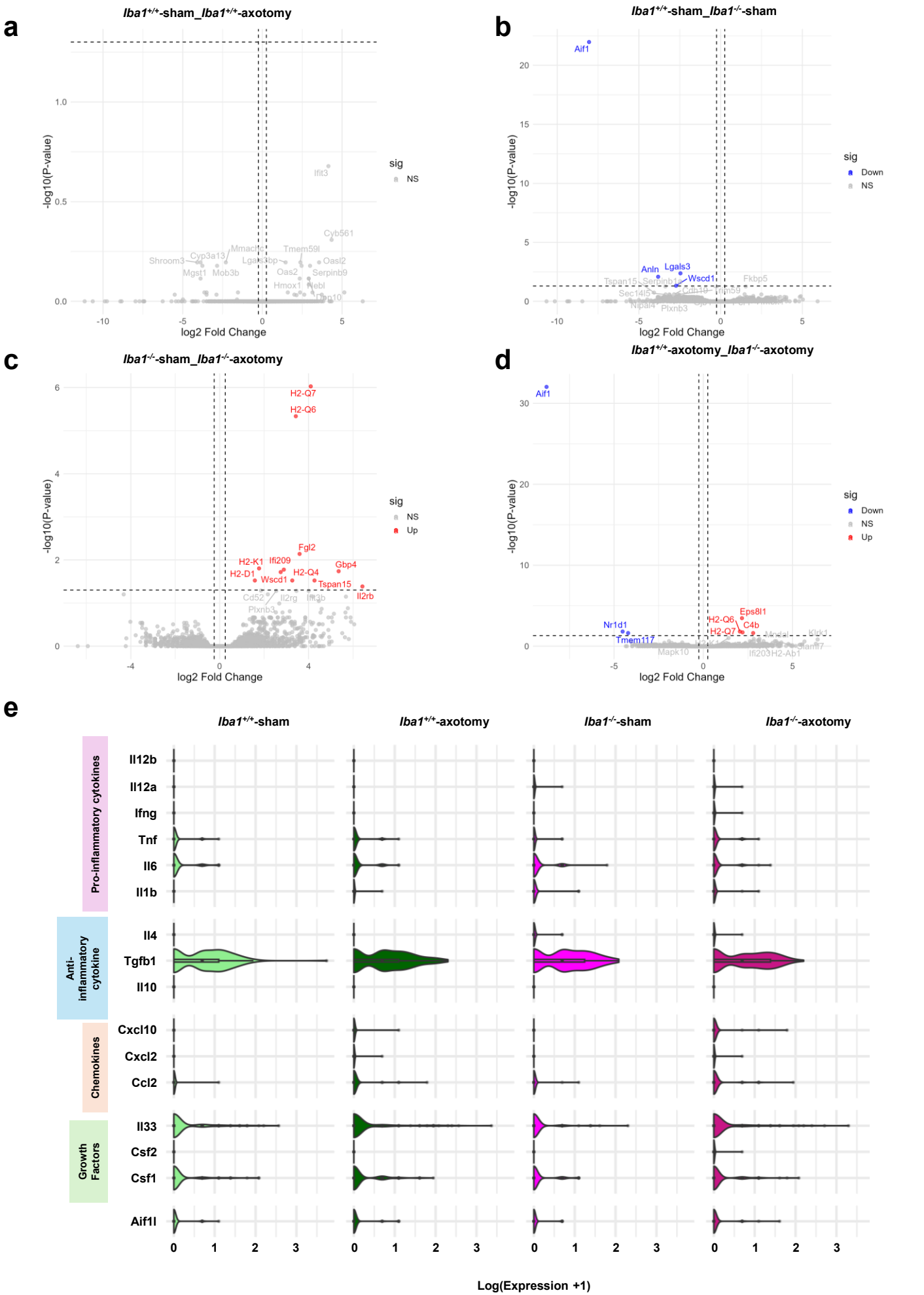
a
Iba1+/+-sham_Iba1+/+-axotomy
-log10(P-value)
log2 Fold Change
sig
NS
Ifit3
Cyb561
Tmem59l
Oasl2
Serpinb9
Oas2
Hmox1
Nebl
Rbp10
Shroom3
Cyp3a13
Mgst1
Mob3b
b
Iba1+/+-sham_Iba1-/--sham
Down
NS
Aif1
Anln
Lgals3
Wscd1
Fkbp5
Tspan15
Sec14l5
Nipal4
Plxnb3
c
Iba1-/--sham_Iba1-/--axotomy
Up
H2-Q7
H2-Q6
Fgl2
H2-K1
Ifi209
H2-D1
Wscd1
H2-Q4
Gbp4
Tspan15
Il2rb
Cd52
Il2rg
Plxnb3
d
Iba1+/+-axotomy_Iba1-/--axotomy
Eps8l1
H2-Q6
C4b
H2-Q7
Nr1d1
Tmem117
Mapk10
Ifi203
H2-Ab1
e
Iba1+/+-sham
Iba1+/+-axotomy
Iba1-/--sham
Iba1-/--axotomy
Pro-inflammatory cytokines
Il12b
Il12a
Ifng
Tnf
Il6
Il1b
Anti-inflammatory cytokine
Il4
Tgfb1
Il10
Chemokines
Cxcl10
Cxcl2
Ccl2
Growth Factors
Il33
Csf2
Csf1
Aif1l
Log(Expression +1)

Figure S12. Differential expression in microglia: volcano plots and cytokine-related gene expression.
(a–d) Volcano plots show $\log_2$ fold change (x-axis) versus $-\log_{10}$(p-value) (y-axis) for each gene. Significantly upregulated genes ($\log_2$FC > 0.25, p < 0.05) are in red, downregulated genes ($\log_2$FC < −0.25, p < 0.05) in blue, and non-significant genes in grey. Dashed lines mark the fold-change thresholds (±0.25) and significance cut-off (p = 0.05). The top 15 most significant genes are annotated in each panel.
(a) *Iba1*$^{+/+}$-sham vs. *Iba1*$^{+/+}$-axotomy: genes upregulated in the *Iba1*$^{+/+}$-axotomy are in red; genes downregulated in the *Iba1*$^{+/+}$-axotomy are in blue.
(b) *Iba1*$^{+/+}$-sham vs. *Iba1*$^{-/-}$-sham: genes upregulated in *Iba1*$^{-/-}$-sham are in red; genes downregulated in *Iba1*$^{-/-}$-sham are in blue.
(c) *Iba1*$^{-/-}$-sham vs. *Iba1*$^{-/-}$-axotomy: genes upregulated in *Iba1*$^{-/-}$-axotomy are in red; genes downregulated in *Iba1*$^{-/-}$-axotomy are in blue.
(d) *Iba1*$^{+/+}$-axotomy vs. *Iba1*$^{-/-}$-axotomy: genes upregulated in *Iba1*$^{-/-}$-axotomy are in red; genes downregulated in *Iba1*$^{-/-}$-axotomy are in blue.
(e) Violin plots of cytokines, chemokines, growth factors, and Aif1l.
Single-cell RNA-seq data (Seurat) display log-transformed expression in each group (*Iba1*$^{+/+}$sham, *Iba1*$^{+/+}$-axotomy, *Iba1*$^{-/-}$-sham, *Iba1*$^{-/-}$-axotomy). Genes are grouped into pro-inflammatory cytokines, anti-inflammatory cytokines, chemokines, growth factors, and Aif1l (a microglial marker). Colors denote groups (light green: *Iba1*$^{+/+}$-sham; dark green: *Iba1*$^{+/+}$-axotomy; magenta: *Iba1*$^{-/-}$-sham; dark pink: *Iba1*$^{-/-}$-axotomy). Horizontal violins show distributions; embedded boxplots indicate medians and interquartile ranges. No statistically significant differences were detected among the four groups for any gene (Kruskal-Wallis test, adjusted p > 0.05).

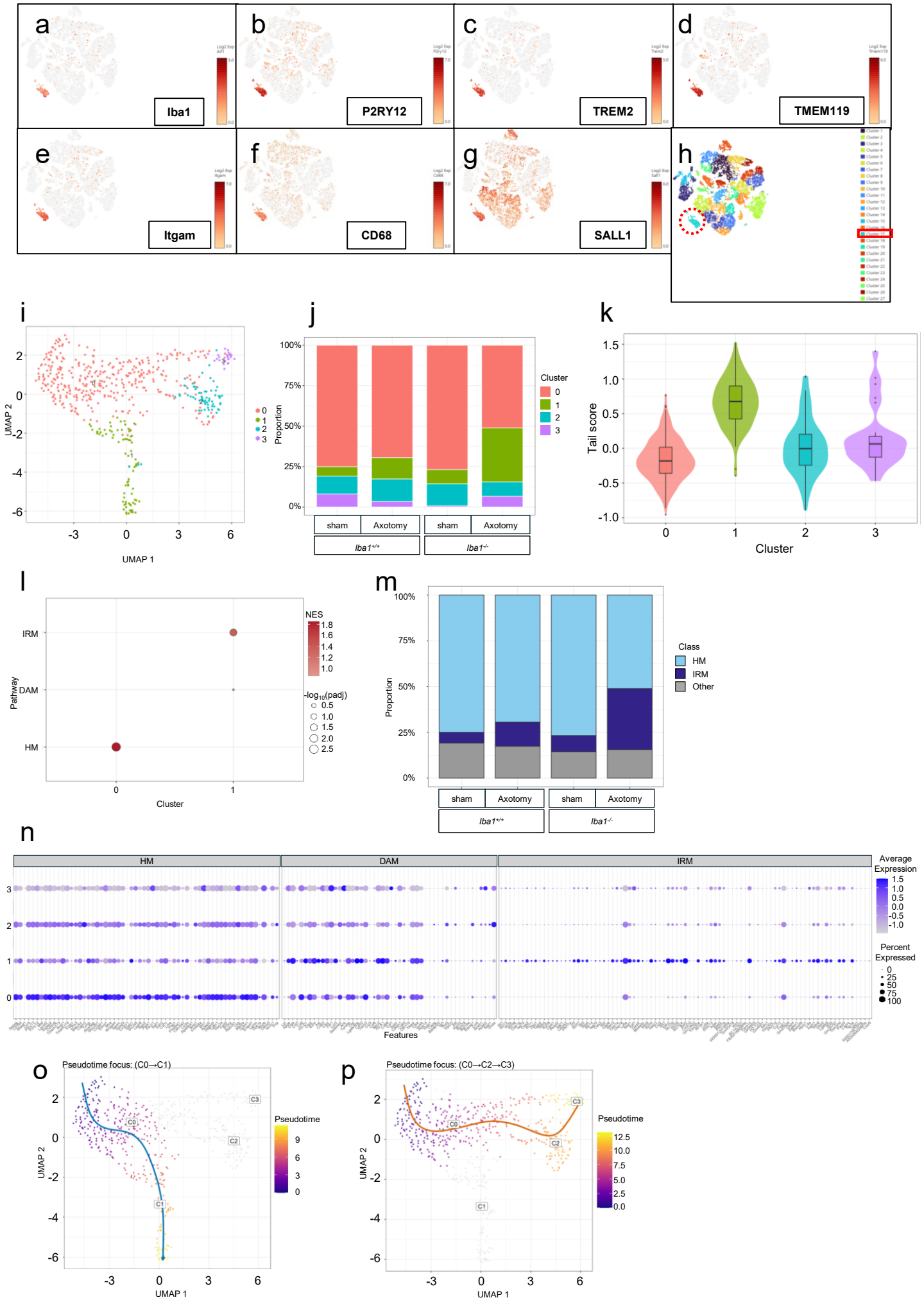
a
Iba1
b
P2RY12
c
TREM2
d
TMEM119
e
Itgam
f
CD68
g
SALL1
h
i
UMAP 2
UMAP 1
j
Proportion
Cluster
sham
Axotomy
lba1+/+
lba1-/-
k
Tail score
Cluster
l
IRM
DAM
HM
Pathway
NES
-log10(padj)
Cluster
m
Proportion
Class
HM
IRM
Other
n
HM
DAM
IRM
Average Expression
Percent Expressed
Features
o
Pseudotime focus: (C0→C1)
Pseudotime
UMAP 2
UMAP 1
p
Pseudotime focus: (C0→C2→C3)
Pseudotime
UMAP 2
UMAP 1

Figure S13. Identification, subclustering, and functional annotation of microglia.
(a–g) UMAP feature maps for canonical microglial markers: (a) Iba1, (b) P2RY12, (c) TREM2, (d) TMEM119, (e) Itgam (CD11b), (f) CD68, and (g) SALL1.
(h) Global UMAP of all nuclei/cells with the microglial population inferred from marker expression (outlined region).
(i) UMAP of the microglial subset after reclustering, resolving four clusters (0–3).
(j) Cluster composition across experimental groups (*Iba1*$^{+/+}$-sham, *Iba1*$^{+/+}$-axotomy, *Iba1*$^{-/-}$-sham, and *Iba1*$^{-/-}$-axotomy) quantified as the fraction of microglial cells assigned to each cluster (stacked bars).
(k) ‘‘Tail’’ module score estimating similarity to axotomy-induced microglial states [1, 2]. For each cell, gene expression was z-scored, the mean of upregulated signature genes was subtracted by the mean of downregulated signature genes, and the scores were summarized by cluster and group. Violin plots depict the score distributions; higher values indicate a stronger resemblance to the axotomy program. Cluster 1 showed the highest enrichment (statistics are reported in the panel).
(l) Bubble color shows NES; bubble size is −log10(FDR). Outlined bubbles indicate FDR < 0.05. Preranked lists were built per cluster (cluster vs. all others). Microglia gene sets were curated and assigned to three programs—homeostatic (HM), DAM, and IRM—following the guidelines in Fumagalli et al., 2025. [3].
(m) Distribution of cells assigned to these program labels per cluster using the classification in Fumagalli et al., 2025. [3].
(n) Dot plot of representative annotation markers underlying the program assignment in Fumagalli et al., 2025. [3] (color, average expression; dot size, % expressing cells).
(o) Trajectory inference on microglia. Slingshot was run on the microglia-only UMAP, with the root fixed to the homeostatic cluster (C0, chosen by the highest HM program score). The thick curve shows the fitted principal curve, and the arrowheads indicate increasing pseudotime. Points are individual cells colored by pseudotime (low, purple → high, and yellow). Grey outlines mark cluster centroids and labels (C0–C3).
(p) The same slingshot fit is overlaid on the shared UMAP to illustrate progression from C0 toward the activated states (passing through/ending in C2–C3). Cells are colored by pseudotime as in (o). Arrows indicate direction along the principal curve. Cluster labels and centroids are shown for reference.

Figure S14. Volcano Plots and GO Enrichment for Microglial Clusters C0–C3
(a, e, i, m) Volcano plots of differentially expressed genes for clusters 0–3 versus the remaining microglia (red, upregulated; blue, downregulated; labeled genes denote top hits; thresholds shown in panels).
(b–d), (f-h), (j-l), (n-p) Gene Ontology / pathway enrichment for the DEG sets from clusters 0–3 (dot size, gene ratio; color, adjusted significance or enrichment score). GO terms: BP (Biological Process), MF (Molecular Function), CC (Cellular Component).

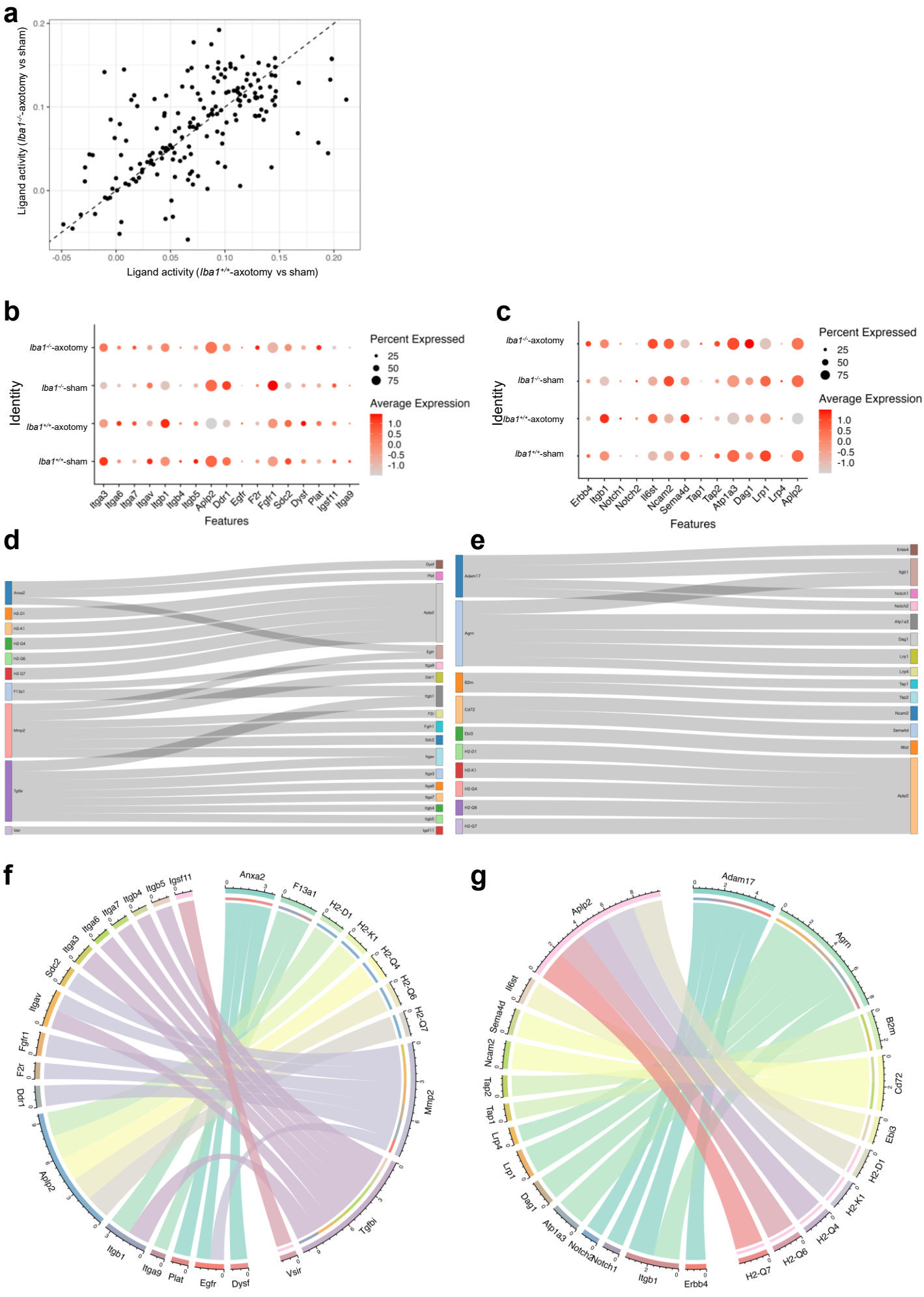
a
Ligand activity (Iba1-/--axotomy vs sham)
Ligand activity (Iba1+/+-axotomy vs sham)
b
Identity
Iba1-/--axotomy
Iba1-/--sham
Iba1+/+-axotomy
Iba1+/+-sham
Itga3 Itga6 Itga7 Itgav Itgb1 Itgb4 Itgb5 Aplp2 Ddr1 Egfr F2r Fgfr1 Sdc2 Dysf Plat Igsf11 Itga9
Features
Percent Expressed
25
50
75
Average Expression
1.0
0.5
0.0
-0.5
-1.0
c
Identity
Iba1-/--axotomy
Iba1-/--sham
Iba1+/+-axotomy
Iba1+/+-sham
Erbb4 Itgb1 Notch1 Notch2 Il6st Ncam2 Sema4d Tap1 Tap2 Atp1a3 Dag1 Lrp1 Lrp4 Aplp2
Features
Percent Expressed
25
50
75
Average Expression
1.0
0.5
0.0
-0.5
-1.0
d
Anxa2
H2-D1
H2-K1
H2-Q4
H2-Q6
H2-Q7
F13a1
Mmp2
Tgfbi
Vsir
Dysf
Plat
Aplp2
Egfr
Itga9
Ddr1
Itgb1
F2r
Fgfr1
Sdc2
Itgav
Itga3
Itga6
Itga7
Itgb4
Itgb5
Igsf11
e
Adam17
Agrn
B2m
Cd72
Ebi3
H2-D1
H2-K1
H2-Q4
H2-Q6
H2-Q7
Erbb4
Itgb1
Notch1
Notch2
Atp1a3
Dag1
Lrp1
Lrp4
Tap1
Tap2
Ncam2
Sema4d
Il6st
Aplp2
f
Anxa2
F13a1
H2-D1
H2-K1
H2-Q4
H2-Q6
H2-Q7
Mmp2
Tgfbi
Vsir
Dysf
Egfr
Plat
Itga9
Itgb1
Aplp2
Ddr1
F2r
Fgfr1
Itgav
Sdc2
Itga3
Itga6
Itga7
Itgb4
Itgb5
Igsf11
g
Adam17
Agrn
B2m
Cd72
Ebi3
H2-D1
H2-K1
H2-Q4
H2-Q6
H2-Q7
Erbb4
Itgb1
Notch1
Notch2
Atp1a3
Dag1
Lrp1
Lrp4
Tap1
Tap2
Ncam2
Sema4d
Il6st
Aplp2

Figure S15. Microglia→ChAT signaling under axotomy: ligand activity, receptor availability, and edge visualizations.
(a) Scatterplot comparing ligand activity scores (*Iba1*$^{+/+}$-axotomy vs. sham on the x-axis; *Iba1*$^{-/-}$ -axotomy vs. sham on the y-axis); the dashed line denotes identity. Each dot is a ligand.
(b–c) Receptor availability in ChAT neurons across groups (rows ordered *Iba1*$^{+/+}$-sham → *Iba1*$^{+/+}$--axotomy → *Iba1*$^{-/-}$-sham → *Iba1*$^{-/-}$-axotomy). Dot size encodes the percentage of expressing cells, and color encodes the scaled mean expression (log-normalized). Panels show two non-overlapping sets of candidate receptors selected from the top ligand–receptor pairs (including integrins and cell-adhesion/ECM-related receptors; see Methods for the full gene list).
(d–e) Sankey diagrams of microglia→ChAT ligand→receptor connections prioritized within genotype (d, *Iba1*$^{+/+}$-; e, *Iba1*$^{-/-}$-; axotomy vs. sham). Link width reflects the aggregate LR weight (pair count or summed evidence, as defined in the Methods). Left nodes are ligands (microglia) and the right nodes are receptors (ChAT).
(f–g) Circular chord diagrams showing the same edges as in d–e (f, *Iba1*$^{+/+}$; g, *Iba1*$^{-/-}$); ribbon width reflects the corresponding LR weight.

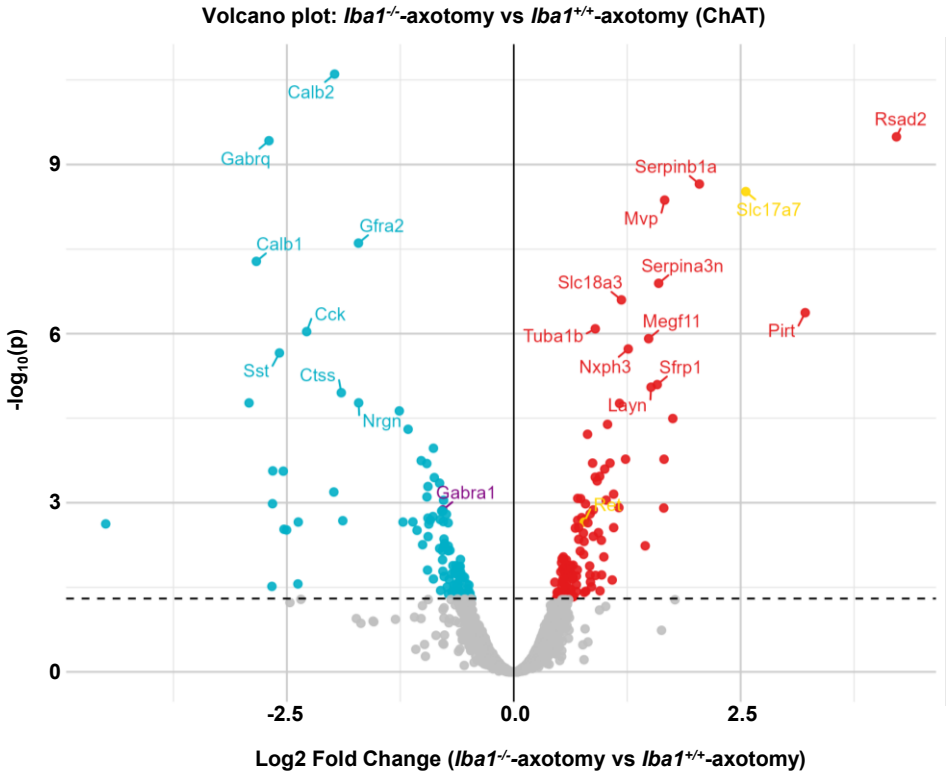

Figure S16. Volcano plot of ChAT⁺ neuronal DEGs (*Iba1*$^{-/-}$-axotomy vs *Iba1*$^{+/+}$-axotomy) identifying Gabra1, VGLUT1, Ret for validation
Volcano plot showing differentially expressed genes in ChAT-positive neurons between *Iba1*$^{-/-}$-axotomy and *Iba1*$^{+/+}$-axotomy groups. Points are colored by regulation: upregulated (red), downregulated (blue), and others (gray). Slc17a7 (VGLUT1) and Ret are highlighted in orange, and Gabra1 in purple.

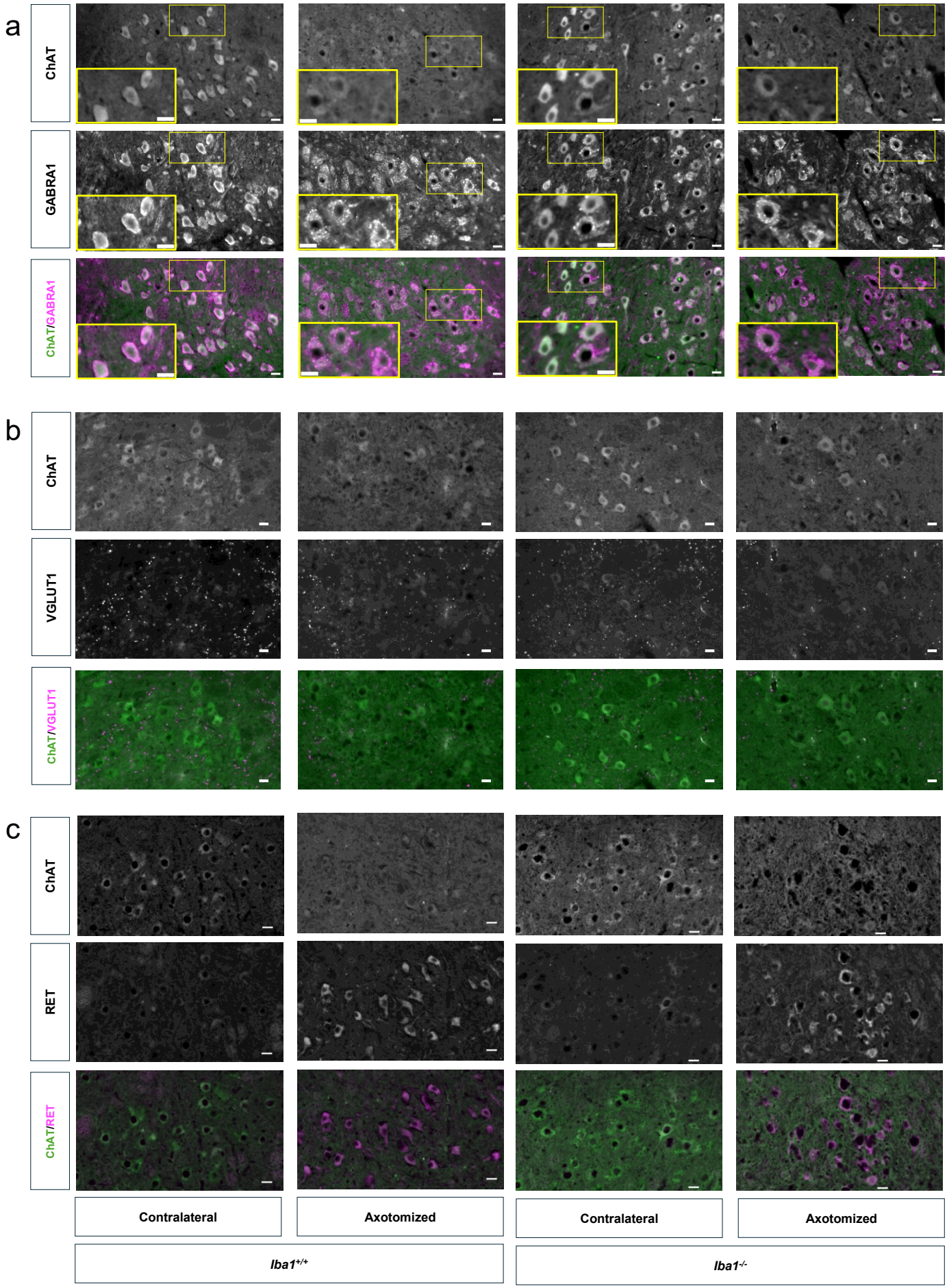

Figure S17. Immunofluorescence analysis of ChAT-positive motoneurons after axotomy.
(a) Representative images of ChAT (green) and GABRA1 (magenta) immunostaining in the facial motor nucleus 7 days after axotomy. Sections from the contralateral and axotomized sides of wild-type (*Iba1*$^{+/+}$) and *Iba1*-deficient (*Iba1*$^{-/-}$) mice are shown.
(b) Representative images of ChAT (green) and VGLUT1 (magenta) immunostaining in the same regions and conditions as in (a).
(c) Representative images of ChAT (green) and RET (magenta) immunostaining under the same experimental conditions.
Scale bars: 20 μm.

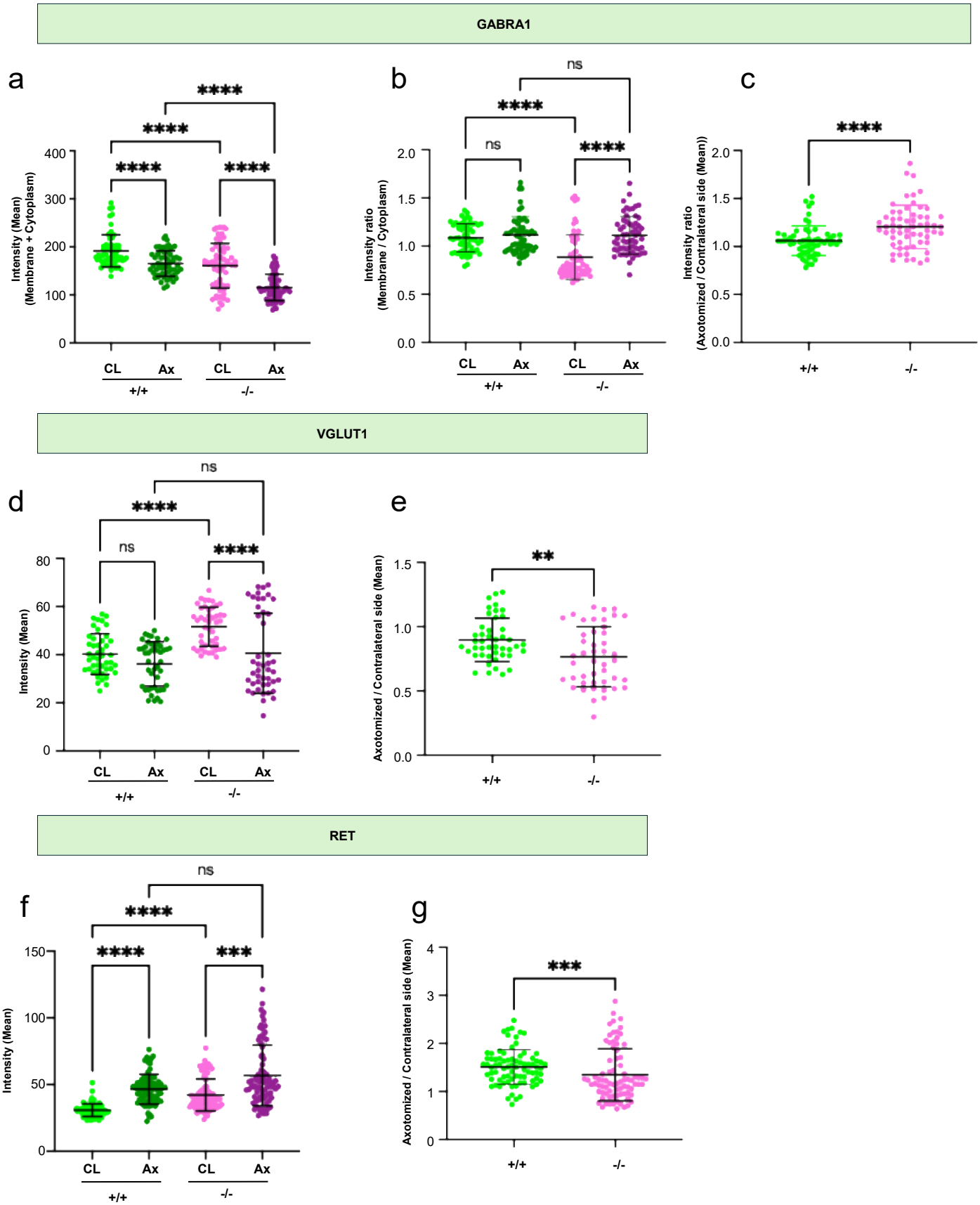

Figure S18. Changes in perisomatic synaptic markers around facial motoneurons 7 days after axotomy.
(a–c) GABRA1 intensity. Facial motor nuclei were analyzed at day 7 post–facial nerve axotomy. For each motoneuron, GABRA1 immunofluorescence was quantified in the soma cytoplasm and in a 3-µm perisomatic membrane ring. Mice: n = 4 per genotype; 15 cells per mouse (60 cells in total).
(a) Sum of cytoplasm + membrane intensities per cell. (b) Membrane/cytoplasm intensity ratio. (c) The ratio in (b) was further normalized as the axotomized/contralateral mean within genotype. Colors: light green, *Iba1*$^{+/+}$-contralateral; dark green, *Iba1*$^{+/+}$-axotomized; magenta, *Iba1*$^{-/-}$-contralateral; maroon, *Iba1*$^{-/-}$-axotomized. In (c), light green = *Iba1*$^{+/+}$ and magenta = *Iba1*$^{-/-}$.
(d–e) VGLUT1 intensity. A circular ROI (diameter 37.9 µm) centered on each motoneuron was used to measure VGLUT1 intensity. Mice: n = 3 per genotype; 15 cells per mouse (45 cells in total).
(d) Raw intensity by side/group (same four-color scheme as above). (e) Axotomized / contralateral mean within genotype. Light green = *Iba1*$^{+/+}$ and magenta = *Iba1*$^{-/-}$.
(f–g) RET intensity. The same 37.9-µm ROI was used to measure RET intensity. Mice: n = 4 per genotype; 20 cells per mouse (80 cells in total).
(f) Raw intensity by side/group (four-color scheme).
(g) Axotomized / contralateral mean within genotype (light green = *Iba1*$^{+/+}$; magenta = *Iba1*$^{-/-}$).
Dots show individual cells with mean ± standard error of the mean. Significance: **p < 0.01, ***p < 0.001, ****p < 0.0001; ns, not significant (two-sided tests; exact procedures in the Supplementary Methods). Abbreviations: ROI, region of interest; *Iba1*$^{+/+}$, wild-type; *Iba1*$^{-/-}$, knockout.

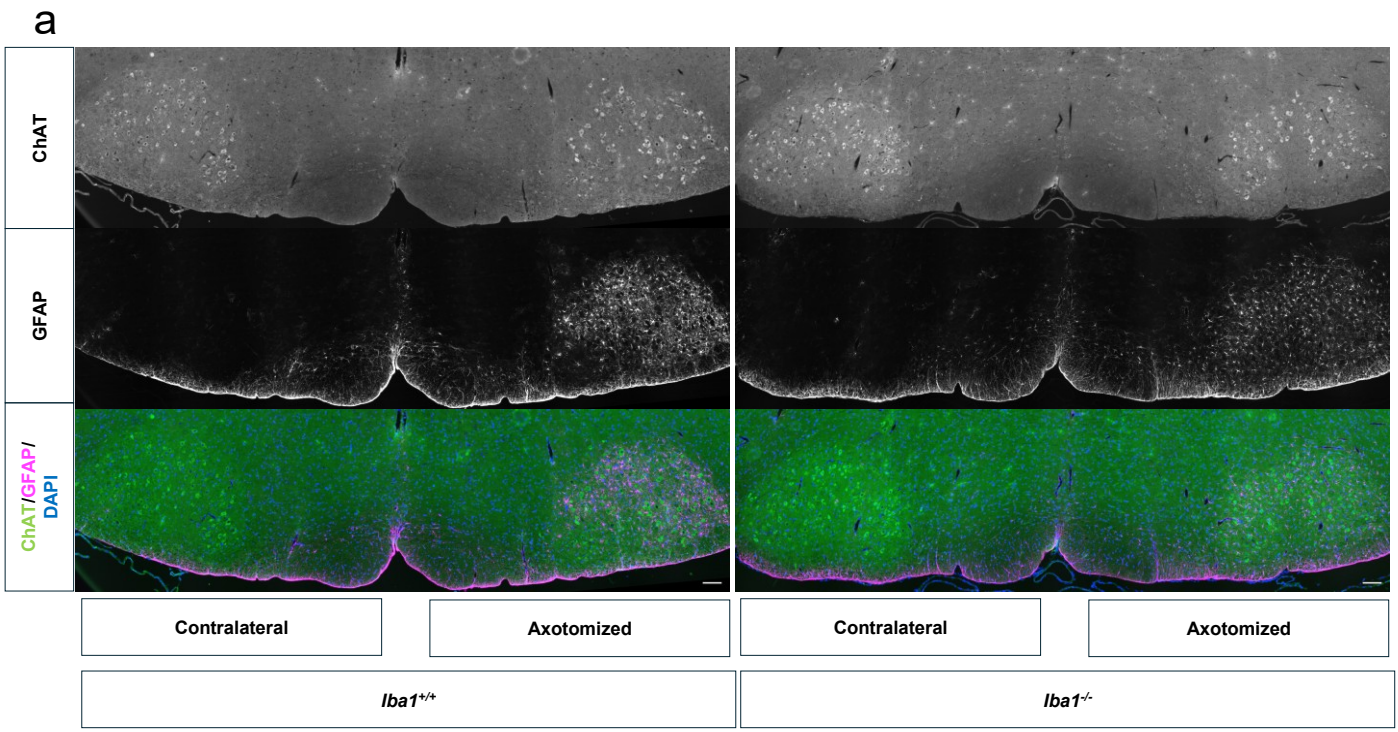

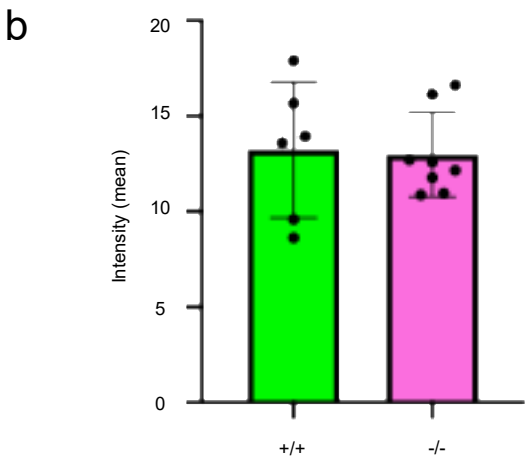

Figure S19. Astrocytic response in the facial motor nucleus 28 days after axotomy
(a) Representative sections of the facial motor nucleus stained for ChAT (green), GFAP (magenta), and DAPI (blue); single-channel grayscale images are shown above, with merged images below. Scale bar = 100 µm.
(b) Quantification of GFAP immunofluorescence in the axotomized facial motor nucleus at 28 dpi. *Iba1*$^{+/+}$ n=6, *Iba1*$^{-/-}$ n=8. No genotype difference. Data are presented as means ± SD. Significance was assessed using an unpaired two-tailed t-test.

Supplemental references

1. Tay, T.L., Sagar, Dautzenberg, J., Grun, D. & Prinz, M. Unique microglia recovery population revealed by single-cell RNAseq following neurodegeneration. *Acta Neuropathol Commun* **6**, 87 (2018).
2. Tay, T.L.*, et al.* A new fate mapping system reveals context-dependent random or clonal expansion of microglia. *Nat Neurosci* **20**, 793-803 (2017).
3. Fumagalli, L.*, et al*. Microglia heterogeneity, modeling and cell-state annotation in development and neurodegeneration. *Nat Neurosci* **28**, 1381-1392 (2025).